AIAA SciTech Forum
8–12 January 2018, Kissimmee, Florida
2018 AIAA Aerospace Sciences Meeting

10.2514/6.2018-0547

Can Flapping Propulsion Boost Airplane Technology? The Flapping-Tail Concept Airplane

Haithem E. Taha*
University of California, Irvine, CA 92697

Flapping propulsion has been deemed inefficient for practical use in thrusting actual airplanes. In this paper, we revisit this claim in the light of several recent findings on the unsteady aero/hydro dynamics of natural flyers/swimmers (e.g., birds, insects, cetaceans). We propose a new airplane concept, called the Flapping-Tail Concept Airplane (FTCA), in which the horizontal tail is driven by a power shaft into a pitching-plunging-flapping motion through a flapping mechanism. For such a concept, we show that there is a significant room for boosting flapping propulsive efficiency that may outperform the current turbofan engine technologies. We use Garrick's classical unsteady aerodynamic model for flapping propulsion to show that allowing for a simultaneous flap deflection with pitching-plunging may enhance the propulsive efficiency by 20%. Moreover, we propose other promising interacting flow mechanisms that may enhance the propulsive efficiency even more and provide a geometric control theoretic formulation to guide such an interaction. We also show the favorable effect of operating in the stall regime with large amplitudes. Finally, we study the effect of such an oscillating tail on the flight mechanics of the airplane and provide recommendations for future investigations necessary to make the proposed vision come closer to real applications.

I. Introduction

Nature designs of flyers are significantly more efficient than man-made ones. For example, the power-to-weight ratio of jet airplanes is about 80 kW/ton versus 16 kW/ton for birds and insects.[1] In fact, mimicking natural creatures (birds) was the first intuitive way humans proposed to achieve man-made flight, which is interestingly rekindled by the efforts of DeLaurier[2] among others. However, the early pioneers, such as Sir George Cayley, realized the necessity of separating lift from propulsion. Indeed, this concept is one of the main pillars underpinning the development of modern airplanes, which was learnt in a hard way through the life-sacrifice of many early explorers. With this lesson in mind, we propose a new airplane concept that is propelled through flapping its tail while the lift is being generated in the conventional way using stationary wings. We call it the Flapping-Tail Concept Airplane (FTCA).

Flapping propulsion has been known to the aeronautical engineering community for long time. However, to the best of our knowledge, it has never been proposed for propelling airplanes; simply because it is deemed inefficient. However, the recent advances on the unsteady aero/hydro-dynamics of birds, insects, and fish have revealed optimum operating conditions over which flapping propulsion can be considerably more efficient than the current state-of-the-art turbo-fan engine technology. Typical values of the propulsive efficiency of high-bypass ratio turbofan engines range between 0.65-0.75.[3] Moreover, the recent advances in turbo engines have lead to 78% propulsive efficiency for the current state-of-the-art technology (e.g., GE CFM56-7B, which is used on the Boeing 737-600/-700/-800/-900). On the other hand, the recent advances on flapping propulsion as an unconventional thrust mechanism resulted in higher propulsive efficiency 87% at relatively high thrust coefficients, even without flow control, as shown experimentally by Triantafyllou and his colleagues[4] on pitching-plunging wings. Moreover, we show in this paper that there is a significant room for improving such a propulsive efficiency by allowing for more flow interacting mechanisms and exploiting unsteady phenomena.

*Assistant Professor, Henry Samueli Career Development Chair, Mechanical and Aerospace Engineering, AIAA Member.

In this paper, we pose an idea rather than tell a full story. The FTCA is investigated from aerodynamic performance and flight mechanics considerations. For this purpose, we use Garrick's model for flapping propulsion,[5] which is based on Theodorsen's classical unsteady aerodynamic theory.[6] Using such a model, we show that adding a simultaneous flap oscillation to a pitching-plunging wing may enhance the flapping propulsive efficiency by 20%. The Boeing 737-800 is used as an illustrative example. It is expected that flapping propulsion can provide up to 25% saving in fuel consumption. This unprecedented enhancement in propulsive efficiency can be achieved by a novel flapping technique that relies on the interaction between different motions of the flapping surface (pitching, plunging, and flapping) and flow controls (suction/blowing and synthetic jets). We propose the geometric control theory to guide such an interaction. Therefore, we present some of its underpinning concepts.

II. Garrick's Classical Model of Flapping Propulsion[5]

Garrick[5] developed a model for the propulsive thrust and efficiency due to a pitching-plunging-flapping flat plate, similar to the one shown in Fig. 1. The model is based on Theodorsen's classical unsteady aerodynamic theory,[6] which basically assumes (i) potential flow, (ii) attached flow, (iii) small disturbance, and (iv) that the Kutta condition is satisfied at the trailing edge. Theodorsen's theory is for a simple harmonic motion

$$\alpha(t) = A_\alpha e^{i\omega t}, \quad h(t) = He^{i\omega t+\phi_h}, \text{ and } \delta(t) = A_\delta e^{i\omega t+\phi_\delta} \tag{1}$$

where ω is the oscillation frequency, A_α, H, and A_δ are the motion amplitudes, and ϕ_h, ϕ_δ represent the phase shift between the pitching motion and the plunging and flapping motions, respectively. Only the final results of Garrick's model[5] will be presented below.

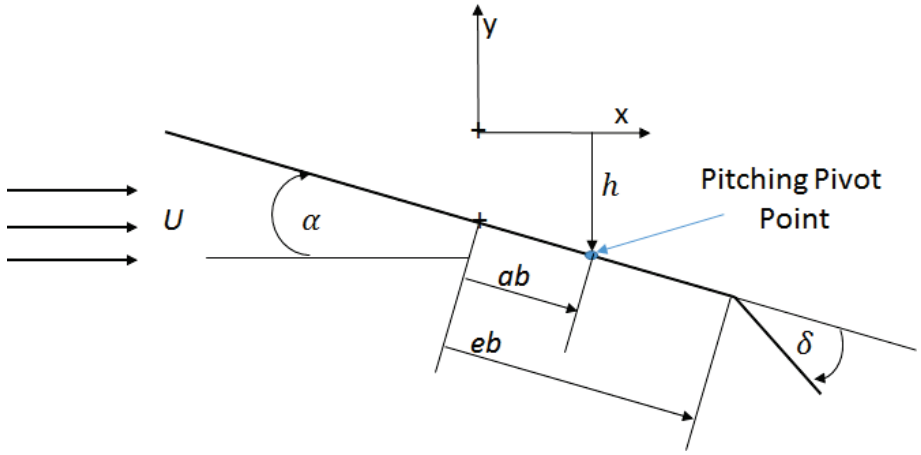

Figure 1. A schematic diagram for an oscillating flat plate.

Consider the oscillating flat plate shown in Fig. 1, where U is the free stream velocity, h is the plunging displacement (positive downward), α is the pitching angle (positive clockwise/pitching up), δ is the flap deflection (positive down), b is the semi-chord length, and ab, eb are the distances from the mid-chord point to the pitching pivot point and flap hinge location, respectively. The main aerodynamic input is the normal velocity at the three-quarter-chord point, as recommended by Pistolesi theorem,[7] pp. 80, which is written (positive downward) as

$$v_{3/4} = U\alpha + \dot{h} + b(1/2 - a)\dot{\alpha} + \frac{T_{10}}{\pi}U\delta + \frac{bT_{11}}{2\pi}\dot{\delta} \tag{2}$$

where small α is assumed and the dot refers to a time-derivative. The first three terms are obvious and the last two terms can be derived in a classical thin airfoil theory fashion. The coefficients T_{10}, T_{11} are among a list of geometric constants that are related to e (representative for the flap-chord ratio), which are given by

$$T_1 = -\frac{1}{3}(2+e^2) \quad \overline{1-e^2} + e\cos^{-1}e, \quad T_2 = e(1-e^2) - (1+e^2) \quad \overline{1-e^2}\cos^{-1}e + (\cos^{-1}e)^2$$

$$T_3 = -\frac{1-e^2}{8}(5e^2+4) + \frac{e}{4}(7+2e^2) \quad \sqrt{1-e^2}\cos^{-1}e - (1/8+e^2)(\cos^{-1}e)^2,$$

$$T_4 = e\sqrt{1-e^2} - \cos^{-1}e, \qquad T_5 = -(1-e^2) + 2e\sqrt{1-e^2}\cos^{-1}e - (\cos^{-1}e)^2$$

$$T_7 = \tfrac{e}{8}(7+2e^2)\sqrt{1-e^2} - (1/8+e^2)\cos^{-1}e, \quad T_8 = -\tfrac{(1-e^2)^{3/2}}{3} - eT_4$$

$$T_9 = \tfrac{1}{2} \quad \tfrac{1}{3}(1-e)^{3/2} + aT_4\Big(, \qquad T_{10} = \sqrt{1-e^2} + \cos^{-1}e$$

$$T_{11} = (2-e)\sqrt{1-e^2}(1-2e)\cos^{-1}e, \quad T_{12} = 2T_4 + T_{11}, \quad T_{13} = -\tfrac{T_7+T_1(e-a)}{2}$$

$$T_{15} = T_4 + T_{10}, \quad T_{16} = T_1 - T_8 - (e-a)T_4 + T_{11}/2, \quad T_{17} = -2T_9 - T_1 + (a-0.5)T_4$$

$$T_{18} = T_5 - T_4T_{10}, \quad T_{19} = T_4T_{11}, \quad T_{20} = T_{10} - 2\sqrt{1-e^2}$$

Based, on this aerodynamic input $v_{3/4}$, Garrick wrote the total normal force N, pitching moment M_α at the pivot, and hinge moment M_δ, corresponding to the three motions h, α and δ, as

$$\begin{aligned} N &= -\rho b^2\Big]\pi\Big)U\dot\alpha + \ddot h - ab\ddot\alpha\Big(- T_4U\dot\delta - bT_1\ddot\delta\sqrt{} - 2\pi\rho bUv_{3/4}C(k) \\ M_\alpha &= -\rho b^2\Big]\pi b\Big)(1/2-a)U\dot\alpha - a\ddot h + (1/8+a^2)b\ddot\alpha\Big(+ T_{15}U^2\delta + T_{16}bU\dot\delta + 2T_{13}b^2\ddot\delta\sqrt{} + \\ &+ 2\pi\rho b^2(1/2+a)Uv_{3/4}C(k) \\ M_\delta &= -\tfrac{\rho b^2}{\pi}\Big]\pi b\Big)T_{17}U\dot\alpha - T_1\ddot h + 2T_{13}b\ddot\alpha\Big(+ T_{18}U^2\delta - \tfrac{T_{19}b}{2}U\dot\delta - T_3b^2\ddot\delta\sqrt{} - \rho T_{12}b^2Uv_{3/4}C(k) \end{aligned} \tag{3}$$

where $k = \frac{\omega b}{U}$ is the reduced (non-dimensional) frequency and $C(k)$ is Theodorsen function (unsteady lift deficiency factor), which is given by[6]

$$C(k) = \frac{H_1^{(2)}(k)}{H_1^{(2)}(k) + iH_0^{(2)}(k)}$$

where $H_n^{(m)}$ is the Hankel function of m^{th} kind of order n. The Theodorsen function represents the frequency response of the unsteady lift dynamics. That is, the multiplication $v_{3/4}C(k)$ is interpreted after writing $v_{3/4}(t) = V_{3/4}e^{i\omega t}$, where $V_{3/4}$ may be complex number, as

$$v_{3/4}C(k) = \Re\ \ V_{3/4}C(k)e^{i\omega t}\Big($$

where $\Re(.)$ denotes the real part of its complex argument. The first terms, between square brackets, in the three equations (3) represent the non-circulatory contributions (added/virtual mass) while the other terms, containing $C(k)$, represent the circulatory ones. Garrick also provided the force on the flap as

$$\begin{aligned} N_\delta &= -\tfrac{\rho b^2}{\pi}\Big]\pi\Big)-T_4U\dot\alpha - T_4\ddot h + bT_9\ddot\alpha\Big(- \tfrac{T_5}{2}U\dot\delta - \tfrac{T_2b}{2}\ddot\delta\sqrt{} + \\ &- \tfrac{\rho b}{\pi}U\sqrt{1-e^2}\Big)\pi b(1-e)\dot\alpha + 2U\sqrt{1-e^2}\delta + b(1-e)T_{10}\dot\delta\Big(- 2\rho bUT_{20}v_{3/4}C(k) \end{aligned} \tag{4}$$

The thrust force T_x is then given by

$$T_x = \pi\rho bS^2 + N\alpha + N_\delta\delta \tag{5}$$

where the first term represents the suction force $S = \lim_{x\to -b}\gamma(x)\sqrt{x+b}$ with γ being the vorticity distribution, which is known to possess a square root singularity at the leading edge ($x = -b$). That is, the suction force S is finite. Garrick showed that S is given by

$$S = \frac{1}{\pi\sqrt{2}}\Big]\pi\ \ 2v_{3/4}C(k) - b\dot\alpha\Big(- 2\quad \sqrt{1-e^2}U\delta + bT_4\dot\delta\sqrt{} \tag{6}$$

Finally, the aerodynamic power required to sustain oscillation is given by

$$P = -\Big)N\dot h + M_\alpha\dot\alpha + M_\delta\dot\delta\Big(\tag{7}$$

As such, the thrust coefficient C_T and propulsive efficiency can be defined as

$$C_T = \frac{\bar T_x}{\rho U^2 b} \quad \text{and} \quad \eta_P = \frac{\bar T_x U}{\bar P}$$

where overbar indicates a cycle-averaged quantity; i.e.,

$$\bar T_x = \frac{\omega}{2\pi}\Big[_0^{2\pi/\omega} T_x(t)dt \quad \text{and} \quad \bar P = \frac{\omega}{2\pi}\Big[_0^{2\pi/\omega} P(t)dt$$

III. Flapping Propulsion and Enhanced Flow Dynamics

The simplicity of Garrick's model[5] allows scrutiny of the flapping propulsion problem, hence drawing fundamental conclusions about the problem. In particular, plunging is significantly more efficient than pitching for propulsion. Plunging alone is thrust producing at any frequency while there is a limited range of frequency corresponding to each pivot location over which positive T_x is achievable via pitching oscillations. For example, if $a = 1/2$ (pitching about the three-quarter-chord point), T_x is negative for all values of ω.

Of particular, interest, the case of pure plunging. It can be shown that, for this case, the averaged thrust force and aerodynamic power required are given by

$$\bar{T}_x = \pi\rho b\omega^2 H^2 |C(k)|^2 \quad \Rightarrow \quad C_T = \pi k^2 \hat{H}^2 |C(k)|^2 \tag{8}$$

resulting in the following important relation for propulsive efficiency in the case of pure plunging

$$\eta_P = \frac{|C(k)|}{\cos \angle C(k)} \tag{9}$$

where $\hat{H} = \frac{H}{b}$.

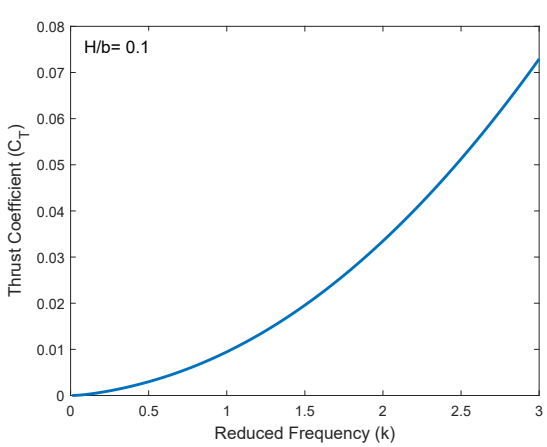

(a) Thrust Coefficient.

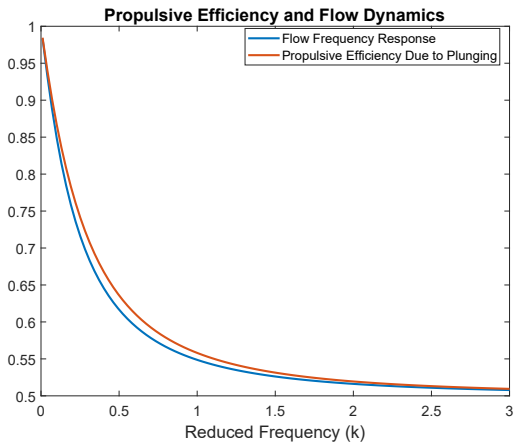

(b) Propulsive Efficiency.

Figure 2. Variations of the thrust coefficient and propulsive efficiency with frequency in the case of pure plunging.

Equations (8,9), which are represented in Fig. 4, clearly tell the story of classical flapping propulsion. First, the variation of the propulsive efficiency with frequency is mainly dictated by the flow dynamical response (i.e., Theodorsen's frequency response function $C(k)$ in the small-disturbance attached flow). Since the angle of $C(k)$ is small and does not vary significantly with frequency (maximum $\angle C(K)$ is about 15 degrees), the variation of η_P with k follows that of $|C(k)|$, as shown in Fig. 2(b). Since, $|C(k)|$ is monotonically decreasing with k, so does η_P resulting in maximum efficiency of 100% at zero frequency and approaches 50% as $k \to \infty$. In addition, the thrust coefficient C_T increases quadratically with k and $\hat{H}$. Note that increasing the latter beyond a certain limit will violate the small disturbance assumption and may physically lead to operation in stall where in either case, Garrick's model and results are not applicable. That is, if more thrust is required, it can be achieved via flapping (plunging) at higher frequencies. However, the higher the frequency is, the lower the propulsive efficiency is. This trade-off between thrust level and efficiency is the main reason why flapping propulsion was abandoned from practical considerations; the high-frequencies needed to achieve a required thrust level typically results in a significantly low propulsive efficiency.

While Garrick's small-disturbance model almost ruled out flapping propulsion from practical applications, as discussed above, the relatively recent water tunnel experiments by Andersen et al.[4] at Reynolds number of $40,000$ revealed different (non-monotonic) variations of η_P with the Strouhal number $St = \frac{2fH}{U} = \frac{k\hat{H}}{\pi}$, as shown in Fig. 3. They considered several cases of pitching-plunging with different amplitudes and phase differences. An optimum propulsive efficiency of 87% was observed simultaneously with $C_T = 0.24$ at $\hat{H} = 0.375$ (relatively large amplitude), $k = 1.17$, $\phi_h = 75°$, and a maximum angle of attack of 21° (operating

in the stall regime). These large amplitude and angles of attack are not applicable to Garrick's model. Hence, the deviation from Garrick's behavior is expected. However, this result indicates the achievement of a decent thrust level $C_T = 0.24$ at a high propulsive efficiency (87%) when using large amplitude-plunging in the stall regime with a specific phase shift between pitch and plunge.

The above finding can be physically explained by recalling the recent investigations of Choi et al.[8] and Zakaria et al.[9] who studied the unsteady flow dynamics in the stall regime. Choi et al.[8] used the immersed boundary method to perform a direct numerical simulation of Navier Stokes equations on a flat plate undergoing a surging motion over the Reynolds number range of 100-500. The authors obtained a Fourier transform of the lift coefficient due to surging at small angles of attack ($\alpha = 5°$) that is close to the potential flow theoretical prediction of Greenberg[10] (analogous to Theodorsen for pitching-plunging). However, they observed a different behavior of the lift spectrum in the stall regime at $\alpha = 15°$. In particular, a peak in the lift spectrum is observed at $k = 0.6 - 0.7$, as shown in Fig. More recently, Zakaria et al.[9] conducted a plunging experiment at $Re = 80,000$ and constructed lift frequency responses analogous to Theodorsen function $C(k)$ at the linear, stall, and post-stall regimes. Despite the difference in airfoil motion (surging versus or plunging) and the operating Reynolds number (500 versus 80,000) between Choi et al.[8] and Zakaria et al.,[9] the latter also observed an enhanced lift dynamics (frequency response) in the stall regime near $k = 0.7$, as shown in Fig. 4(b). In fact, the authors of both efforts attributed such enhancement in the lift amplitude to the same reason; to synchronization between the motion frequency and leading edge vortex (LEV) shedding time-scale such that the changes in the LEV lift and the quasi-steady lift are coincident. It is interesting to note that this optimum range of frequency closely matches the results of Wang.[11] She performed a numerical simulation for the Navier-Stokes equations to study impulsively started flows and plunging oscillations of a two dimensional wing section. Similar to the experimental results of Dickinson and Gotz,[12] her numerical simulations showed that the steady-state lift, reached after the impulsive start, cannot remain indefinitely constant at high angles of attack because of the well known LEV instability for two-dimensional flows (i.e., in the absence of a stabilizing axial or spanwise flow); a Von Karman street starts to emerge after about 10 chord lengths of travel. Wang[11] concluded that there is a lift-optimum time interval for plunging; between the instant at which the steady state lift is reached (after the Wagner's transient response dies out[13]) and before the spawn of the first Von Karman street vortex pair. It is also noteworthy to mention other efforts that pointed to similar lift enhancement mechanisms.[14–16]

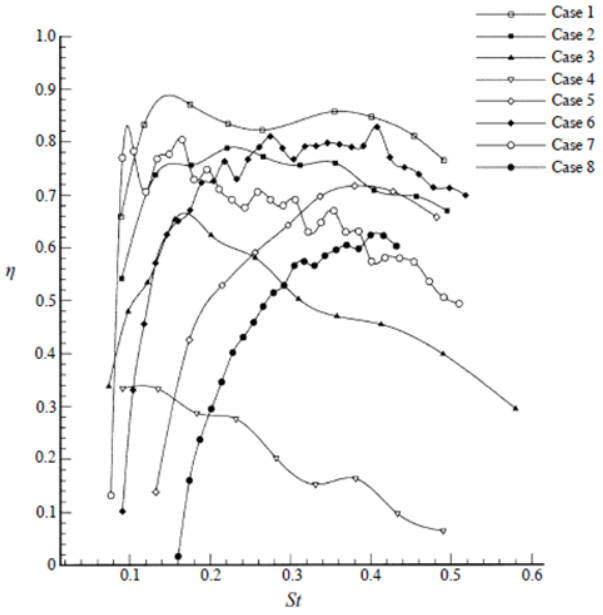

Figure 3. Variation of the propulsive efficiency with Strouhal number St for a pitching-plunging airfoil in a water tunnel at Reynolds number of 40,000. Adopted from Andersen et al.[4]

Recall that the propulsive efficiency due to flapping is mainly dictated by the unsteady flow dynamical response ($C(k)$ in the linear range), as shown in Fig. 2(b). Consequently, the recent advances on unsteady aerodynamics, presented above, that showed enhanced flow dynamical response near stall, may suggest an optimum flapping propulsion in that region. In fact, it may also explain the enhanced flapping propulsion observed by Anderson et al.[4] when operating in the stall regime.

IV. An Illustrative Example: Boeing 737-800

Consider the Boeing 737-800 during cruise. Assume that there exists a mechanical transformer converting the engine power into an oscillating mechanism connected to a wing-shaped surface (e.g., the horizontal tail). Aside from the skeptical questions that may arise about the feasibility of such a high-risk idea, the two imperative questions that need to be addressed immediately are (i) Can it generate enough thrust to

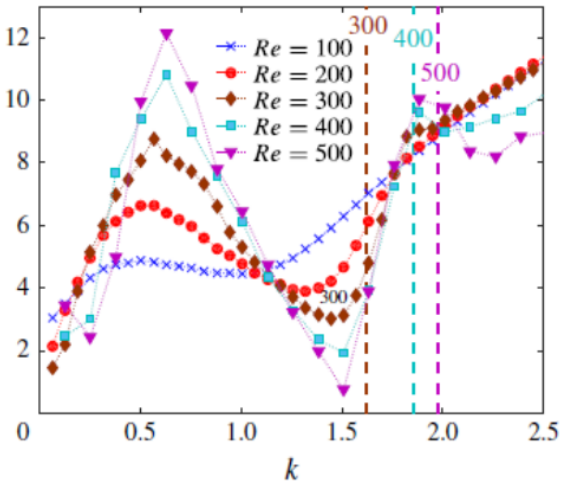

(a) Adopted from Choi et al.[8]

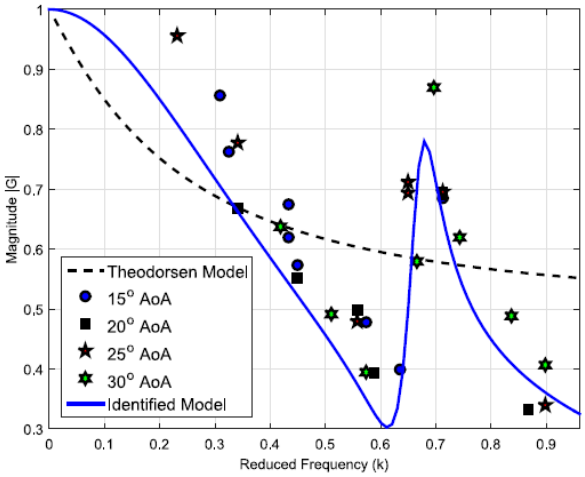

(b) Adopted from Zakaria et al.[9]

Figure 4. Enhanced flow dynamics in the stall regime for surging flat plate at small Reynolds numbers[8] and for plunging NACA 0012 at $Re = 80,000$.

overcome the whole airplane drag? and (ii) Is it more efficient than the best-in-class technology? Recalling the specifications and some of the aerodynamic performance characteristics of the Boeing 737-800, as given by Perkins et al.[17] and presented here in Table 1, the first question can be easily answered through the following rough calculations. The cruise lift and drag coefficients are simply given by

$$C_L = \frac{2W_{MTO}}{\rho U^2 S} = 0.51 \quad \text{and} \quad C_D = C_{D_0} + KC_L^2 = 0.0331$$

where Table 1 provides values of the maximum take-off weight W_{MTO}, the wing reference area S, and the drag polar parameters C_{D_0}, K. At an altitude of $30,000ft$, the air density is $0.4592kg/m^3$ and speed of sound is $303.1m/s$ resulting in a forward speed $U = 238m/s$. As such, the required thrust coefficient C_T based on the oscillating surface area (i.e., horizontal tail in this example) is given by

$$C_T = \frac{S}{S_t}\left(C_D - C_{D_t}\right) = \frac{S}{S_t} C_D \left(1 - C_{D_t}/C_D\right) = 0.12$$

where S_t is the horizontal tail reference area and C_{D_t}/C_D is the horizontal tail drag contribution to the whole airplane drag in cruise; both are given in Table 1. Hence, the required thrust coefficient (0.12) is quite achievable by pitching-plunging surfaces, as shown in many results in literature (see the review of Rozhdestvensky and Ryzhov[1]): Maximum experimentally-verified flapping C_T values range between 1.0-1.5, which is significantly higher than the 0.12 requirement. In fact, the thrust coefficient corresponding to the optimum propulsive efficiency obtained by Anderson et al.[4] was 0.24, which is double the required value.

As for the efficiency question, we use Garrick's classical model of flapping propulsion,[5] presented in Sec. II above, to solve the following optimization problem

$$\max_{\boldsymbol{\chi}} \eta_P : \quad \text{subjet to } C_T = 0.12 \text{ and } \boldsymbol{\chi} \in \mathcal{X}$$

where $\boldsymbol{\chi}$ is a vector of design variables and $\mathcal{X}$ is the optimization set (set of admissible variables). That is, the problem is to maximize the propulsive efficiency η_P subject the thrust constraint $C_T = 0.12$, which is enough to overcome the whole airplane drag during cruise. The second constraint is to ensure the design variables are within the physical bounds and/or abiding by the small-disturbance assumption to ensure the validity of the used model of Garrick. Note that confining the search for such a narrow region using this linearized model, it is not expected to obtain a high propulsive efficiency at this thrust level; the high propulsive efficiency observed by Anderson et al.[4] was by operating in the stall regime with a large plunging amplitude, which are outside of our feasible search domain (set of admissible variables) because of the limitation of Garrick's model.

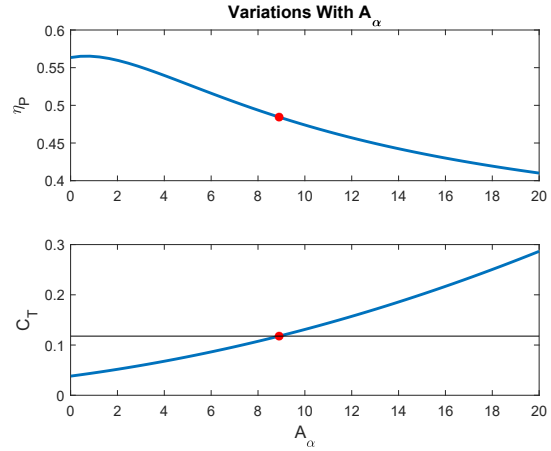

(a) Variations With A_α.

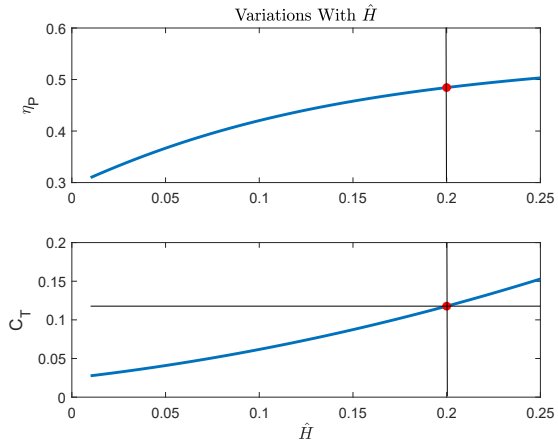

(b) Variations With $\hat{H}$.

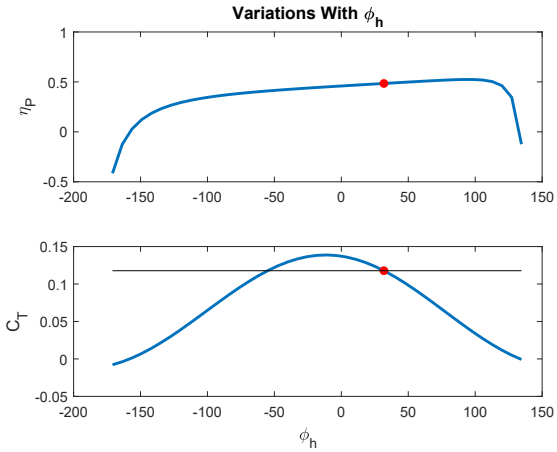

(c) Variations With ϕ_h.

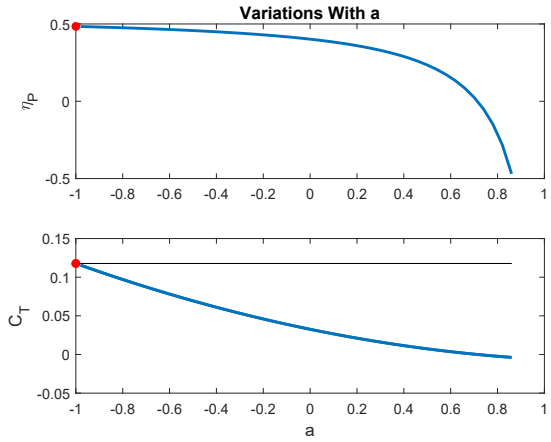

(d) Variations With a.

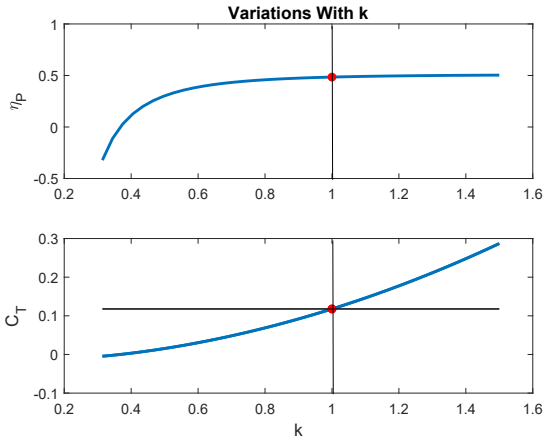

(e) Variations With k.

Figure 5. Variations of η_P and C_T with the design variables near the optimum point for the pitching-plunging case. The optimum design point is marked in a red star.

Specification/Performance Characteristic	Value
Cruise Mach number & altitude	0.785 & 30,000 ft
Wing reference area S & mean aerodynamic chord chord $\bar{c}$	1255.16 ft^2 & 12.39 ft
Horizontal tail reference area S_t & mean aerodynamic chord $\bar{c}_t$	352.84 ft^2 & 8.68 ft
Maximum take off weight W_{MTO}	174,200 lb.
Drag Polar	$C_{D_0} = 0.0241$ and $K = 0.0376$
Horizontal tail drag contribution to the whole airplane drag in cruise	$C_{D_t}/C_D = 5.4\%$
Lift curve	$C_{L_0} = 0.13$ and $C_{L_\alpha} = 7.71$ /rad
Pithing moment of inertia I_y	$2.76 \times 10^7 slug/ft^3$
Pitching stability coefficients	$C_{M_\alpha} = -5.9/rad$ and $C_{M_q} = -106.94$.
Horizontal tail moment arm ℓ_t	55 ft

Table 1. Specifications and aerodynamic performance characteristics of the Boeing 737-800.[17]

We solve two versions of the above optimization problem. The first one is for a pitching-plunging flat plate where $\boldsymbol{\chi}$ includes five design variables: $\boldsymbol{\chi} = [A_\alpha, \hat{H}, \phi_h, a, k]^T$. The second problem is for pitching-plunging-flapping flat plate where $\boldsymbol{\chi}$ includes eight design variables: $\boldsymbol{\chi} = [A_\alpha, \hat{H}, \phi_h, a, k, A_\delta, \phi_\delta, e]^T$ subject to one additional constraint $e > a$. Matlab sequential quadratic programming is used to solve the posed optimization problems. Many random initial points in the design space are used to avoid local minima. Table 2 shows the lower and upper bounds of the design variables and the optimum values for each problem; $\boldsymbol{\chi}_1^*$ for the pitching-plunging case and $\boldsymbol{\chi}_2^*$ for the pitching-plunging-flapping case.

Design Variable	Lower Bound	Upper Bound	Optimum Value $\boldsymbol{\chi}_1^*$	Optimum Value $\boldsymbol{\chi}_2^*$
Pitching Amplitude A_α°	0	15°	8.9°	15°
Plunging Amplitude $\hat{H}$	0	0.2	0.2	0.2
Pitching-Plunging Phase ϕ_h°	−180°	180°	31.8°	55.3°
Pitching Pivot Location a	-1	1	-1	-1
Reduced Frequency k	0	1	1	1
Flapping Amplitude A_δ°	0	25°	–	17.5°
Pitching-Flapping Phase ϕ_δ°	−180°	180°	–	−174.7°
Flapping Hinge Location e	-1	1	–	0.21
Optimum η_P			48.4%	67.0%

Table 2. Lower and upper bounds of the design variables and the optimum solution for each optimization problem.

The upper limits of the pitching and plunging amplitudes (A_α and $\hat{H}$) are set to confine the feasible space to relatively small amplitudes. The upper limit of the flapping frequency, represented by k, is set to unity here, where in reality, it will be dictated by practical considerations. The upper limit of the flap deflection A_δ is set to 25°, which is a typical practical limit for an airplane control surface deflection.

Figure 5 shows variations of the propulsive efficiency and thrust coefficient with the design variables for the pitching-plunging case. One design variable is considered at a time, while the other variables held constant at the optimum value from Table 2. The optimum design point is also shown as a red star. Studying these variations, we observe that the optimizer pushed some of the design variables to their boundaries such as $\hat{H}$, a, and k because of the monotonic variation of η_P with such variables. Other variables (A_α and ϕ_h) are dictated by the thrust constraint; i.e., achievable higher values for η_P are sacrificed to satisfy the thrust constraint.

Figure 6 shows variations of the propulsive efficiency and thrust coefficient with the design variables for the pitching-plunging-flapping case. Similar trends to the pitching-plunging case are observed. For example, some design variables are pushed to their boundaries such as A_α, $\hat{H}$, a, and k while others are dictated by

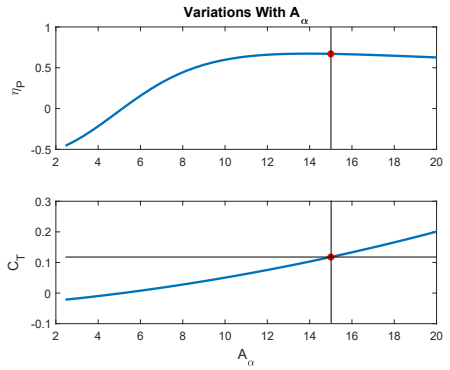

(a) Variations With A_α.

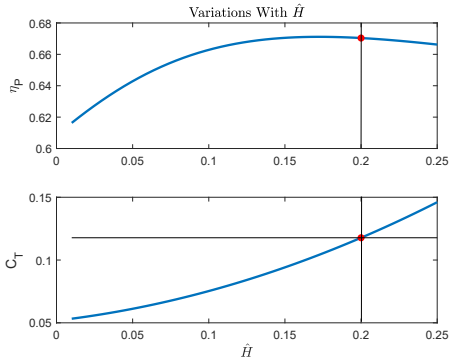

(b) Variations With $\hat{H}$.

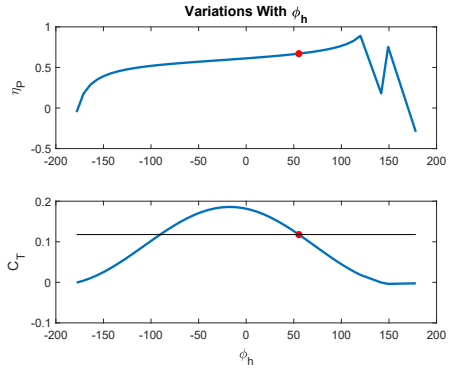

(c) Variations With ϕ_h.

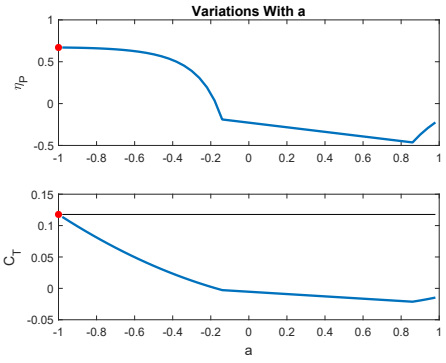

(d) Variations With a.

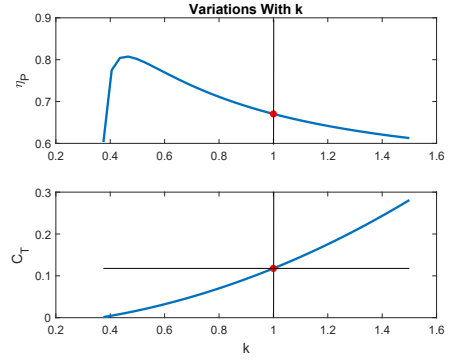

(e) Variations With k.

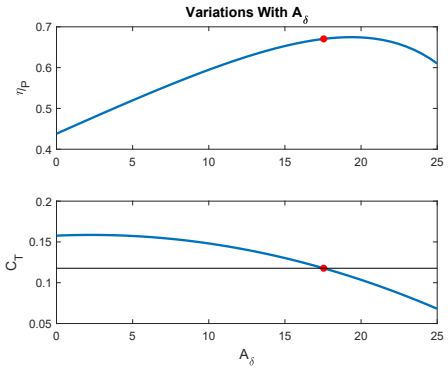

(f) Variations With A_δ.

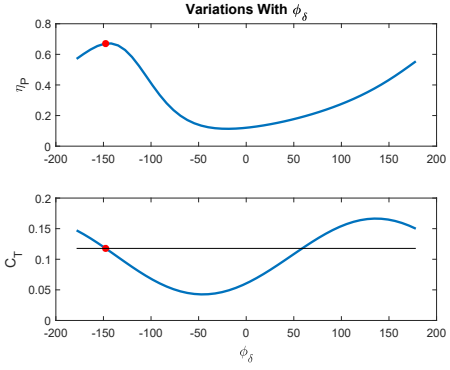

(g) Variations With ϕ_δ.

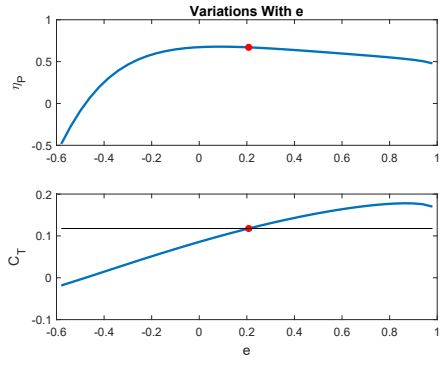

(h) Variations With e.

Figure 6. Variations of η_P and C_T with the design variables near the optimum point for the pitching-plunging-flapping case. The optimum design point is marked in a red star.

the thrust constraint such as ϕ_h. However, unlike the pitching-plunging case, some design variables are set by the optimizer to attain a truly local maximum value for η_P or close, such as A_δ, ϕ_δ and e; namely the additional design variables from the flap deflection. That is, it seems as if pitching-plunging design variables were set to satisfy the thrust constraint while the additional flapping design variables were set free allowing for true optimization of the objective function η_P, which explains the significant enhancement in propulsive efficiency in the flapping case in comparison to the pitching-plunging case; 20% enhancement in η_P.

Several conclusions can be drawn from the solved optimization problems. First, congruent with the fundamental knowledge on flapping propulsion, the optimizer always saturates the plunging amplitude and frequency; i.e., generating most of the thrust by plunging is more efficient. Second, moving the pivot point towards the leading edge is favorable in both cases, which is also consistent with the well-known aerodynamic fact that the effective angle of attack is that of the three-quarter-chord point (Pistolesi theorem). Therefore, in order for the optimizer to maximize the effect of *rotational circulation*,[18,19] the pivot point should be the farthest from the three-quarter-chord point. Third, and more importantly for the theme of this paper is the fact that, just allowing for an interaction with a flap deflection boosts the maximum propulsive efficiency by 20%. We also remark that we did not even exploit the enhanced flow dynamics in the stall regime in this analysis. Therefore, it is expected that allowing for interaction with more flow control mechanisms while availing of the unconventional unsteady flow dynamics in the stall regime will boost the propulsive efficiency even more. To shed some light on how interaction with other flow control mechanisms can be neatly achieved, we present in the next section a quick review on how the mathematically-elegant differential geometric control theory can be used for such an objective.

V. Flow Interacting Mechanisms and Geometric Control Theory

A. Differential Geometric Control Theory

Geometric control theory is a mathematical control theory concerned with dynamical systems evolving on curvy spaces (can also be abstract objects) called *manifolds*. This covers a fairly large class of mechanical systems (e.g., all systems having rotational degrees of freedom). Adopting this geometric view for these dynamical systems requires an appropriate mathematical tool to perform calculus on curvy spaces; that is the differential geometry. One can loosely say that geometric control theory is the intersection of differential geometry and control theory of dynamical systems. The mathematical abstraction of geometric control theory has lead to interesting non-intuitive results beyond linear analysis of stability and controllability. We present below two of these potentials capabilities of the theory.

1. *Nonlinear Controllability and Unconventional Force Generation*

Controllability of a dynamical system is the ability to steer the system from an initial configuration to an arbitrary final configuration in finite time. For linear, time-invariant systems

$$\dot{\boldsymbol{x}}(t) = \boldsymbol{A}\boldsymbol{x}(t) + \boldsymbol{B}\boldsymbol{u}(t),\ \boldsymbol{x} \in \mathbb{R}^n \tag{10}$$

controllability is quite easy to check. The system (10) is completely controllable if and only if[20]

$$\text{rank}\ \ \boldsymbol{B}, \boldsymbol{A}\boldsymbol{B}, ..., \boldsymbol{A}^{n-1}\boldsymbol{B}\Big(= n$$

For nonlinear autonomous systems, controllability is inspected locally at a given point $\boldsymbol{x}_0$. Consider the following finite-dimensional, nonlinear, control-affine system

$$\dot{\boldsymbol{x}}(t) = \boldsymbol{f}(\boldsymbol{x}(t)) + \sum_{j=1}^{m} \boldsymbol{g}_j(\boldsymbol{x}(t))u_j(t),\ \boldsymbol{x} \in \mathbb{M}^n \tag{11}$$

where $\boldsymbol{x}$ is the state vector evolving on an n-dimensional Manifold $\mathbb{M}^n$, $\boldsymbol{f}$ is the drift vector field (uncontrolled dynamics), $\boldsymbol{g}_j$'s represent the control vector fields corresponding to the inputs u_j's. One straight forward, and even sufficient, approach to check controllability of the control-affine nonlinear system (11) at a given point $\boldsymbol{x}_0 \in \mathbb{M}^n$ is to linearize the nonlinear dynamics around $\boldsymbol{x}_0$. Then, controllability of the linearized system can be easily inspected using the controllability check for linear systems. This condition is sufficient; if the linearized system is controllable, then the nonlinear system is locally controllable from $\boldsymbol{x}_0$. However, this

condition is not necessary. **That is, there exists a class of systems that are not linearly controllable but nonlinearly controllable**. In other words, the linear analysis may deem the system (11) uncontrollable and, as such, some attainable states might be deceptively considered not reachable. However, the geometric nonlinear analysis may still prove full controllability for the same system.

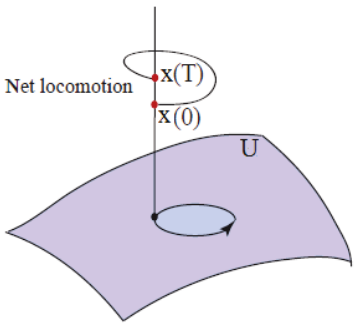

Figure 7. Net motion in the state space due to a Lie bracket operation realized by a periodic change in the control space U.

The main idea is that there can be no direct actuation leading to motion in a prescribed direction, though specific manipulation of the available actuators/controls may generate forces in that missed direction. This concept is generally referred to as *anholonomy*[21] or *geometric phases*.[22,23] For example, for driftless systems ($\boldsymbol{f} = \boldsymbol{0}$), one can generate motion along the vector $\boldsymbol{g}_k$ by turning on the control input u_k and turning off all other controls. Geometric control theory provides us with additional and non-intuitive directions to move along. These directions are determined through *Lie bracket* operations between the different control vectors. The Lie bracket between the two vectors $\boldsymbol{g}_j$ and $\boldsymbol{g}_k$ is defined as

$$[\boldsymbol{g}_j, \boldsymbol{g}_k] = \frac{\partial \boldsymbol{g}_k}{\partial \boldsymbol{x}} \boldsymbol{g}_j - \frac{\partial \boldsymbol{g}_j}{\partial \boldsymbol{x}} \boldsymbol{g}_k$$

If the Lie bracket $[\boldsymbol{g}_j, \boldsymbol{g}_k]$ of two input vector fields is linearly independent of the two generating vectors $\boldsymbol{g}_j$, $\boldsymbol{g}_k$, then the implication is that through some manipulation of the corresponding control inputs u_j, u_k, one can generate motion along a *new* direction; unactuated direction (over which there is no direct control authority). This is particularly useful to recover nonlinear controllability if linear controllability is lost. The motion along some Lie bracket vector $[\boldsymbol{g}_j, \boldsymbol{g}_k]$ can be realized by an out-of-phase periodic signals for the corresponding inputs u_j and u_k.[24–26] A graphical illustration for a net motion in the state space produced via a Lie bracket operation (periodic changes in the control space) is shown in Fig. 7.

At an operating point of interest $\boldsymbol{x}_0$, the space spanned by the iterated Lie brackets between $\boldsymbol{f}$ and $\boldsymbol{g}_j$'s is defined as

$$\Delta(\boldsymbol{x}_0) = \text{span}\left\{\boldsymbol{f}, \boldsymbol{g}_1, ..., \boldsymbol{g}_m, [\boldsymbol{f}, \boldsymbol{g}_1], ..., [\boldsymbol{f}, \boldsymbol{g}_m], [\boldsymbol{f}, [\boldsymbol{f}, \boldsymbol{g}_1]], ...\right\}(\boldsymbol{x}_0) \tag{12}$$

Roughly speaking, If $\Delta(\boldsymbol{x}_0)$ covers the whole tangent space $\mathbb{R}^n$, then the system is accessible from $\boldsymbol{x}_0$;[27–31] that is, the system can be driven to some neighborhood around $\boldsymbol{x}_0$; equivalently, the reachable set from $\boldsymbol{x}_0$ has a non-empty interior. This condition is referred to as the Lie Algebraic Rank Condition (LARC).

2. *Periodic Excitation and Unconventional Force Generation*

Another approach for generating forces/motion in unactuated directions is to use high-frequency, oscillatory control inputs.[23] This is based on the geometrical mechanics fact that an oscillatory control input, though with zero mean, can lead to a net motion.[23,32] In fact, by using the pioneering work of Sarychev,[33] Vela,[34] and Bullo[35] that combine geometric control and averaging theory by exploiting chronological calculus tools of Agrachev and Gamkrelidze,[36] the author and his colleagues[37] have recently shown that the effects of an oscillatory control input u_k on the averaged dynamics of (11) can be represented by the iterated Lie bracket $[\boldsymbol{g}_k, [\boldsymbol{f}, \boldsymbol{g}_k]]$.

Following Bullo[35] with some sloppiness and passing up many details, the *symmetric product* $< \boldsymbol{g}_j : \boldsymbol{g}_k >$ between the two input vectors $\boldsymbol{g}_j$ and $\boldsymbol{g}_k$ is defined as

$$< \boldsymbol{g}_j : \boldsymbol{g}_k > = < \boldsymbol{g}_j : \boldsymbol{g}_k > \triangleq [\boldsymbol{g}_j, [\boldsymbol{f}, \boldsymbol{g}_k]] = [\boldsymbol{g}_k, [\boldsymbol{f}, \boldsymbol{g}_j]$$

Symmetric products can be realized by high-frequency, high-amplitude oscillatory inputs. If $u_j = \omega U_j \cos \omega t$ with high enough ω, the averaged dynamics of the system (11) is written as[34,35,37]

$$\dot{\bar{\boldsymbol{x}}} = \boldsymbol{f}(\bar{\boldsymbol{x}}) - \sum_{j,k=1}^{m} \frac{U_j U_k}{4} < \boldsymbol{g}_j : \boldsymbol{g}_k > (\bar{\boldsymbol{x}}) \tag{13}$$

where over-bar indicates an averaged quantity. The symmetric product vector $< \boldsymbol{g}_k : \boldsymbol{g}_k >$ associated with the input u_k may have a considerably different structure than the input vector field $\boldsymbol{g}_k$. For example, an input vector field $\boldsymbol{g}_k$ may have a zero component in some direction, indicating lack of control authority along that direction. However, the corresponding component of $< \boldsymbol{g}_k : \boldsymbol{g}_k >$ may not vanish indicating the ability to generate a new nonintuitive motion/acceleration (force) in that direction through periodic oscillation of the corresponding control input u_k. The author and his colleagues[37–39] have used the above tools to analyze the nonlinear time-periodic dynamics of hovering insects and flapping-wing micro-air-vehicles. It has been shown that the symmetric product corresponding to back and forth flapping wing can generate an upward vertical force (lift) for the whole body and, hence, balance the flapping vehicle/insect at hover, in spite of the vehicle's inability to directly generate vertical forces.

B. Geometric Control formulation of Unsteady Aerodynamics and Nonlinear Interactions

The above discussion motivates developing a reduced-order model for the unsteady aerodynamics of oscillatory airfoils in the stall regime in the form of Eq. (11); i.e.,

$$\begin{aligned} \dot{\boldsymbol{x}} &= \boldsymbol{f}(\boldsymbol{x}) + \boldsymbol{g}_h(\boldsymbol{x})\ddot{h} + \boldsymbol{g}_\alpha(\boldsymbol{x})\ddot{\alpha} + \boldsymbol{g}_\delta(\boldsymbol{x})\ddot{\delta}(t) + \boldsymbol{g}_s(\boldsymbol{x})\delta_s + \boldsymbol{g}_{sb}(\boldsymbol{x})\delta_{sb} \\ \boldsymbol{y} &= \boldsymbol{\mathcal{H}}\Big)\boldsymbol{x}, \ddot{h}, \ddot{\alpha}, \ddot{\delta}, \delta_s, \delta_{sb}\Big(\end{aligned} \tag{14}$$

where $\boldsymbol{x}$ is a vector of internal aerodynamic states and $\boldsymbol{y}$ is the vector of output variables (e.g., lift and drag coefficients). The vectors $\boldsymbol{g}_h$, $\boldsymbol{g}_\alpha$, $\boldsymbol{g}_\delta$, $\boldsymbol{g}_s$, $\boldsymbol{g}_{sb}$ are the input vector fields associated with plunging, pitching, flap deflection, synthetic jet δ_s, and suction/blowing inputs δ_{sb}, respectively. The synthetic jet δ_s and suction/blowing δ_{sb} inputs are added to allow for more interactions between different flow control mechanisms, as recommended from the previous sections. Then the reduced-order model (14) will allow using constructive techniques from geometric mechanics and control theory, as presented above, to uncover potential unconventional mechanisms to generate forces. For example, the Lie bracket $[\boldsymbol{g}_\delta, \boldsymbol{g}_s]$ will represent the effect of an interaction between a flap deflection and a synthetic jet input, that may not be seen directly in $\boldsymbol{g}_\delta$ and $\boldsymbol{g}_s$ separately or even their linear combinations. Initial efforts that are related to similar, though linear, reduced order modeling can be found in the work of Zakaria et al.[9] and Hemati et al.[40]

VI. Free Energy in the Wake

Another unsteady phenomena that can be exploited to boost the performance of the FTCA is capturing the free energy in the wing wake. To shed some light on this potential, we recall the interesting efforts of Liao and his colleagues.[41,42] Liao et al.[41] studied how trouts modify their body and tail kinematics to swim in the wake of a bluff body (e.g., cylinder). They found that the trout body amplitudes and curvatures are much larger in the presence of Von Karman vortices shed behind a cylinder than those of a trout those of trout swimming at an equivalent flow velocity in the absence of a cylinder. They called this kinematics the *Krmn gait*. They also found that the tail-beat frequency matches the shedding frequency of the cylinder. It is interesting to note that the trout chose to be in the slower flow velocity offered behind a cylinder and modified its body kinematics to synchronize with the shed vortices; such a mechanism may not be propulsive on its own (i.e., in the absence of vortices). These results suggest that fish can capture energy from vortices generated by the environment.

Liao[42] found that the trout muscle activities are reduced when swimming in the wake of a bluff body (i.e., Karman gait). To further investigate this behavior, he placed a dead trout in the wake of a bluff body. He found that the dead trout was able to swim with zero input energy. The Von Karman vortices shed behind the bluff body *naturally* excites the flexible body of the trout and results in kinematics that are thrust producing. As a result, the trout swims forward with zero input energy. This behavior implies a propulsive efficiency that is more than 100%; due to capturing the free energy in the wake. In other words, this result provides a passive thrust generation mechanism in oscillating flows, which can be seen in the interesting video in Ref.[43] Projecting on the proposed FTCA, the tail is oscillating in the wing wake. Therefore, the tail kinematics may be designed to exploit the free energy in the wing wake similar to the Karman gait observed by Liao and his colleagues.[41,42]

VII. Effect on Flight Mechanics

The proposed propulsion mechanism is expected to have a significant effect on flight mechanics, although the oscillation occurs at very high frequencies in comparison to the the airplane flight mechanics modes (e.g., short period and Dutch roll modes). However, such an effect has to be studied. In this section, we adapt Garrick's model, presented in Sec. II, to couple the unsteady aerodynamics of the oscillating horizontal tail with a quasi-steady aerodynamic model for the body flight dynamics. Only longitudinal flight dynamics is considered here.

A. Quasi-Steady Rigid-Body Longitudinal Flight Dynamics

The well-known set of equations governing the longitudinal rigid-body flight dynamics of conventional aircraft is written as[44]

$$\begin{pmatrix} \dot{u} \\ \dot{w} \\ \dot{q} \\ \dot{\theta} \end{pmatrix} = \begin{pmatrix} -qw - g\sin\theta \\ qu + g\cos\theta \\ 0 \\ q \end{pmatrix} + \begin{pmatrix} \frac{1}{m}X \\ \frac{1}{m}Z \\ \frac{1}{I_y}M \\ 0 \end{pmatrix} \tag{15}$$

where g is the gravitational acceleration; m and I_y represent the body mass and moment of inertia about the pitching axis, respectively. The state variables include the forward and normal (positive downward) velocity components (u and w) of the body center of mass, the body pithing angular velocity q, and pitching angle θ. The generalized forces X, Z, and M are the forward and normal forces and pitching moment, respectively, which are given by

$$\begin{pmatrix} X \\ Z \\ M \end{pmatrix} = \begin{pmatrix} L\sin\alpha_b - D\cos\alpha_b + T_{x_{\text{tot}}} \\ -L\cos\alpha_b - D\sin\alpha_b + N_{\text{tot}} \\ M_a + N_{\text{tot}}\ell_t \end{pmatrix} \tag{16}$$

where L and D are the lift and drag forces on the airplane without the horizontal tail, which are given by

$$\begin{aligned} L &= \tfrac{1}{2}\rho V_T^2 S C_L, \quad & C_L &= C_{L_0} + C_{L_\alpha}\alpha_b \\ D &= \tfrac{1}{2}\rho V_T^2 S C_D, \quad & C_D &= C_{D_0} + K C_L^2 \end{aligned} \tag{17}$$

where $V_T = \sqrt{u^2 + w^2}$ is the total airspeed and $\alpha_b = \tan^{-1}\frac{w}{u}$ is the body angle of attack. In Eq. (16), $T_{x_{\text{tot}}}$ and N_{tot} represent the total unsteady thrust and normal forces delivered by the oscillating horizontal tail, which are given by

$$T_{x_{\text{tot}}} = \frac{1}{2}\rho V_T^2 S C_T = \frac{T_x S_t}{\bar{c}_t} \quad \text{and} \quad N_{\text{tot}} = \frac{N S_t}{\bar{c}_t}$$

where T_x is the thrust per unit span on the oscillating tail given in Eq. (5), C_T is the thrust coefficient, and N is the normal force (positive downward) per unit span on the oscillating tail, which will be given below. Finally, the aerodynamic pitching moment M_a is given by

$$M_a = \frac{1}{2}\rho V_T^2 S\bar{c}\Big) C_{M_\alpha}\alpha_b + C_{M_q}\frac{2U}{\bar{c}}q\Big($$

where the wing and tail aerodynamic moments at their respective aerodynamic centers are fairly neglected with respect the significant term $N_{\text{tot}}\ell_t$ in this preliminary study.

B. Unsteady Aerodynamic Model of the Oscillating Tail

Garrick's potential-flow model, presented in Sec. II, is used to to couple the unsteady aerodynamics of the oscillating horizontal tail with the quasi-steady rigid-body flight dynamic model presented above. However, the inputs to Garrick model have to be modified to account for the aerodynamic-dynamic interaction; i.e., the effect of the body motion on the aerodynamics of the oscillating tail. As such, we have the following kinematics of the oscillating tail

$$\begin{aligned} \alpha(t) &= A_\alpha\sin\omega t + \alpha_b, & \dot{\alpha}(t) &= A_\alpha\omega\cos\omega t + q, & \ddot{\alpha}(t) &= -A_\alpha\omega^2\sin\omega t \\ h(t) &= H\sin(\omega t + \phi_h), & \dot{h}(t) &= H\omega\cos(\omega t + \phi_h) + w + q\ell_t, & \ddot{h}(t) &= -H\omega^2\sin(\omega t + \phi_h) \\ \delta(t) &= A_\delta\sin(\omega t + \phi_\delta), & \dot{\delta}(t) &= A_\delta\omega\cos(\omega t + \phi_\delta), & \ddot{\delta}(t) &= -A_\delta\omega^2\sin(\omega t + \phi_\delta) \end{aligned} \tag{18}$$

That is, the body motion (represented by u, w, and q) induces an angle of attack on the horizontal tail $\alpha_b = \tan^{-1}\frac{w}{u}$, a plunging effect (i.e., $\dot{h}$ effect) of $w + q\ell_t$, where the body acceleration terms, $\dot{w}$ and $\dot{q}$, are definitely neglected with respect to the oscillatory acceleration terms $\ddot{\alpha}$, $\ddot{h}$, $\ddot{\delta}$ of the horizontal tail.

Adopting the definitions in Eq. (18), the tail kinematic variables lose periodicity, as the body motion variables are not necessarily periodic, particularly during maneuvering or transient periods. Therefore Garrick's model needs to be generalized for arbitrary time-variation of the aerodynamic inputs (motion variables). The non-circulatory terms in Garrick's model are algebraic; that is, applicable to any set of kinematics. However, the circulatory terms (multiplying $C(k)$) are necessarily for a harmonic input ($v_{3/4}$). As such, these terms have to be generalized for an arbitrary time-varying $v_{3/4}(t)$. Several efforts have been exerted in literature to achieve such an objective; i.e., develop a state space representation of Theodorsen's or Wagner's function, particularly for the latter because, unlike Theodorsen's, it does not even have a closed-form expression. We adopt here Jones approximation[45] for Wagner's function $\phi(s)$

$$\phi(t) = 1 - A_1 e^{-c_1 t} - A_2 e^{-c_2 t} \tag{19}$$

where the constants A_1, A_2, c_1, and c_2 are given by

$$A_1 = 0.165, \quad A_2 = 0.335, \quad c_1 = 0.0455\frac{U}{b}, \quad \text{and} \quad c_2 = 0.3\frac{U}{b}$$

Wagner function represents the lift response due to a unit step change in the angle of attack, or $v_{3/4}$. As such, a transfer function can be constructed by taking the Laplace transform of $\phi(t)$ and dividing by $1/s$, which yields a two-state approximation for Theodorsen function in the Laplace domain as

$$C(s) = \frac{b_2 s^2 + b_1 s + b_0}{s^2 + a_1 s + a_0} \tag{20}$$

where the transfer function coefficients are given by

$$b_2 = 1 - A_1 - A_2, \quad b_1 = c_1 + c_2 - A_1 c_2 - A_2 c_1, \quad b_0 = c_1 c_2, \quad a_1 = c_1 + c_2, \quad \text{and} \quad a_0 = c_1 c_2$$

As such, a two-state unsteady aerodynamic representation is written as

$$\begin{aligned} \frac{d}{dt}\begin{pmatrix} x_{a_1}(t) \\ x_{a_2}(t) \end{pmatrix} &= \begin{bmatrix} 0 & 1 \\ -a_0 & -a_1 \end{bmatrix}\begin{pmatrix} x_{a_1}(t) \\ x_{a_2}(t) \end{pmatrix} + \begin{bmatrix} 0 \\ 1 \end{bmatrix} v_{3/4}(t) \\ y_a(t) &= \begin{bmatrix} b_0 - b_2 a_0 & b_1 - b_2 a_1 \end{bmatrix}\begin{pmatrix} x_{a_1}(t) \\ x_{a_2}(t) \end{pmatrix} + b_2 v_{3/4}(t) \end{aligned} \tag{21}$$

where x_{a_1}, x_{a_2} are internal aerodynamic states, y_a is the aerodynamic output, and $v_{3/4}$ is the aerodynamic input, which is given in Eq. (2) with replacing U by V_T.

Based on the unsteady aerodynamic state space model in Eq. (21), the unsteady aerodynamic loads N, N_δ, and S acting on the oscillating tail due to the kinematics given in Eq. (18) are given by

$$\begin{pmatrix} N \\ N_\delta \\ S \end{pmatrix} = \begin{bmatrix} 0 & -\pi\rho b^2 V_T & \rho b^2 T_4 V_T & \pi\rho a b^3 & \rho b^3 T_1 & -\pi\rho b^2 \\ -\frac{2\rho b}{\pi}(1-e^2)V_T^2 & C_{22} & C_{23} & -\rho b^3 T_9 & \frac{\rho b^3 T_2}{2\pi} & 0 \\ -\frac{\sqrt{2(1-e^2)}}{\pi}V_T & -\frac{b}{\sqrt{2}} & \frac{bT_4}{\sqrt{2}\pi} & 0 & 0 & 0 \end{bmatrix}\begin{pmatrix} \delta \\ \dot{\alpha} \\ \dot{\delta} \\ \ddot{\alpha} \\ \ddot{\delta} \\ \ddot{h} \end{pmatrix} + \begin{bmatrix} -2\pi\rho b V_T \\ -2\rho b T_{20} V_T \\ \sqrt{2} \end{bmatrix} y_a \tag{22}$$

where

$$C_{22} = \rho b^2 (T_4 - (1-e)\sqrt{1-e^2})V_T \quad \text{and} \quad C_{23} = \frac{\rho b^2}{2\pi}(T_5 - 2T_{10}(1-e)\sqrt{1-e^2})V_T$$

and T_x still follows the same definition given in Eq. (5).

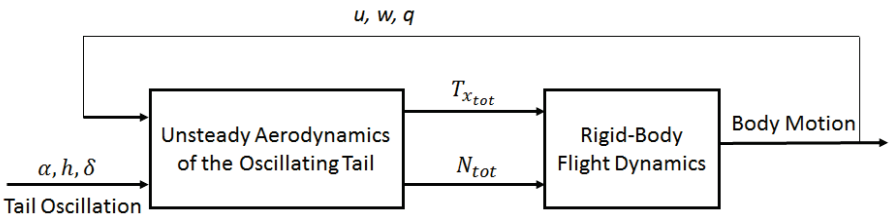

Figure 8. A schematic diagram for the coupled unsteady aero-flight dynamics.

C. Simulation Results

We first consider trim for a straight and level horizontal flight at $u = U$ and zero w, q, and θ. That is, the airplane axes are set such that $w = 0$ at a body angle of attack α_0 that is required to achieve the cruise lift coefficient $C_L = 0.51$. As such, α_b in Eq. (17) is replaced by $\alpha_0 + \alpha_b$. Then, the *averaged* trim equations at $u = U$, $w = 0$, $q = 0$, $\theta = 0$ are given by

$$\begin{array}{rcl} \bar{T}_{x_{tot}} & = & \frac{1}{2}\rho U^2 S \;\; C_{D_0} + K C_L^2 \Big(\\ \bar{N}_{tot} & = & \frac{1}{2}\rho U^2 S C_L - W_{MTO} \\ \bar{N}_{tot}\ell_t & = & 0 \end{array} \tag{23}$$

Note that at pure cruise ($u = U$, $w = 0$, $q = 0$, and $\theta = 0$), the harmonic kinematics (1) yields $\bar{N}_{tot} = 0$. Consequently, the third equation is automatically satisfied and the second equation results in the cruise lift coefficient $C_L = 0.51$ whose drag coefficient is balanced by the averaged thrust due to the oscillating tail. That is, averaged trim is ensured when using the kinematic variables coming from the solved optimization problem. Figure 8 shows a schematic diagram for the tight coupling between the unsteady aerodynamics of the oscillating tail and body flight dynamics (i.e., aerodynamic-dynamic interactions).

Figure 9 shows the response of the coupled unsteady aero-flight dynamic model described above when starting from the initial point $u = U$, $w = 0$, $q = 0$, and $\theta = 0$. One may conclude that the *averaged* trim is not sufficient as the airplane finally and slowly reached an ascent equilibrium. This deviation from cruise is not attributed to the lack of generated thrust. In fact, more thrust is generated than required, which is evident from the initial increase in the speed followed by final climb. Therefore, the deviation from cruise is attributed to the aerodynamic-dynamic interaction between the body motion and the unsteady aerodynamic loads, which leads to a shift in the equilibrium state. In fact, this phenomenon was also observed by the authors and his colleagues[37,46,47] when studying the time-periodic flight dynamics of insects and flapping-wing micro-air-vehicles; the periodic forcing interacts with the time-varying dynamics resulting in a constant drift in the higher-order averaged dynamics. This constant drift, in turn, changes the equilibrium state of the system. This phenomenon is referred to as direct/parametric interaction by Nayfeh and Mook.[48] The resolution of such an issue necessitates periodic shooting algorithms to capture the equilibrium *periodic orbit*, as shown by Hassan and Taha.[49,50] Having said that, it is noteworthy to point to the smooth slowly-varying (low-frequency) response of the airplane despite the applied periodic forcing. The variations shown in Fig. 9 give no clue that they come from periodic forcing. Indeed, the oscillating frequency of the tail is too high to affect the flight mechanics of the airplane beyond the trim issue discussed above.

VIII. Future Recommendations and Impact on Economic Prosperity

The potential of flapping propulsion to advance airplane technology has been discussed. In particular, light has been shed on how a flapping system can boost the propulsive efficiency through (i) large amplitude oscillations in the stall regime, (ii) allowing for more interactions with flow control mechanisms and using the geometric control theory to guide such nonlinear interactions, (iii) capturing the free energy in the wing wake. However, these concepts have been demonstrated for low Reynolds number flight far below the operating range of actual airplanes or even mini unmanned air vehicles. Therefore, first, the presented concepts have to be studied at higher Reynolds number and in the transonic regime. In fact, this study will worth for its own scientific merit. Second, the whole premise, particularly the second point, heavily

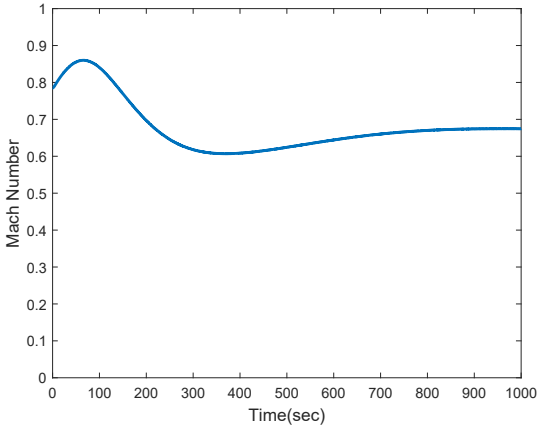

(a) Mach Number.

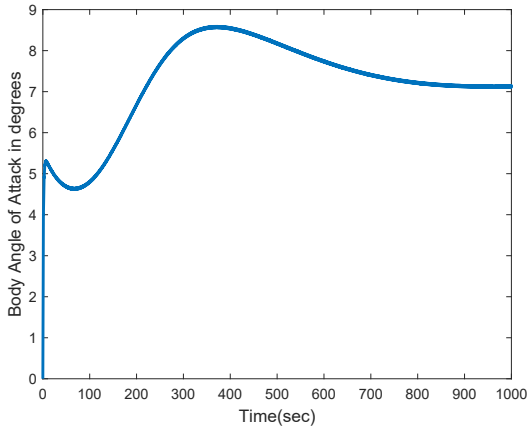

(b) Angle of Attack α_b.

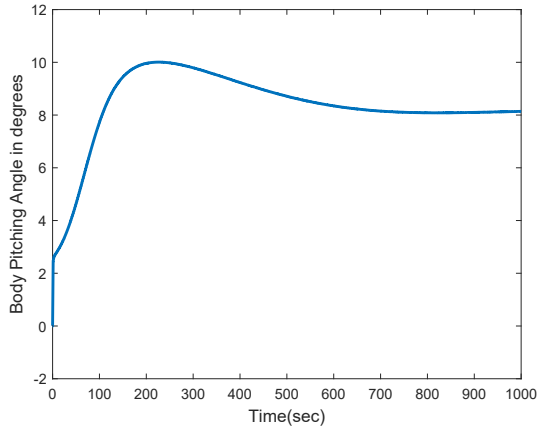

(c) Pitching Angle θ.

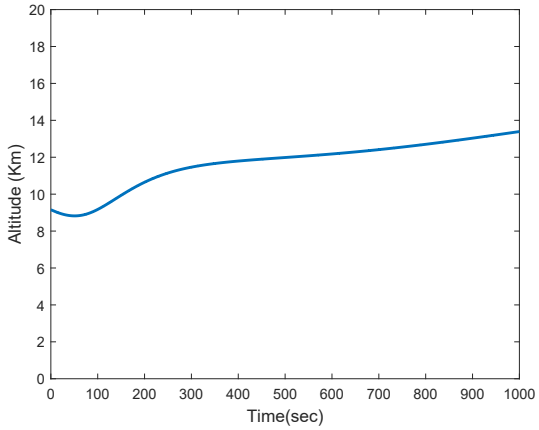

(d) Altitude.

Figure 9. Coupled unsteady aero-flight dynamic simulations.

relies on the development of the reduced-order model (14), which seems to be elusive, particularly in the transonic regime. Therefore, more efforts from the community should be directed towards such an objective as it does not only serve unsteady flapping propulsion but also proper aeroelasticity, flight dynamics, and control analyses, in addition to preliminary design of unconventional airplanes that make use of unsteady aerodynamics. Third, a significant challenge, which is skipped in this initiatory paper, is the structural dynamics of the oscillating tail and the concomitant structural penalty. This study is instrumental for the practicality of the proposed FTCA.

If Triantafyllou and his colleagues[4] managed to demonstrate 87% propulsive efficiency by just flapping in the stall regime with large amplitudes (i.e., only making use of the first point above), then by performing kinematic optimization, allowing for more flow interactions, and capturing energy from the wing wake, one can boost the flapping propulsive efficiency even beyond. It is expected that a flapping propulsive efficiency of 90-95% can be demonstrated by exploiting the unsteady phenomena mentioned above. This enhancement in propulsive efficiency will simply lead to a 20-25% saving in fuel consumption according to the rough estimate

$$\frac{\dot{m}_F}{\dot{m}_{TF}} = \frac{C_D - C_{D_t}}{C_D} \frac{\eta_{P,TF}}{\eta_{P,F}},$$

where the left hand side represents the ratio of the fuel consumption in the FTCA to that of a conventional airplane powered by a turbo-fan engine and $\frac{\eta_{P,TF}}{\eta_{P,F}}$ is the ratio between the turbo-fan engine propulsive efficiency (taken here to be 78% of the state-of-the-art engine GE CFM56-7B) and flapping propulsive efficiency.

This significant splash (25% fuel saving) is not expected in the very saturated aeronautical engineering domain. In fact, saving fuel consumption by one or two percent is already a formidable challenge that, if successfully overcome, will save billions of dollars for airliners as well as saving our environment. Just to give the reader an idea about how saturated airplane designs are and how effective "little" savings can be, the American Airlines decided to replace the paper flight manual (35 lb weight) with an iPad and estimated a 1.2 million dollar savings per year due to such a decision. The introduction of winglets, which save about 5% in fuel consumption, remarks a revolution in airplane performance that saved more than 5 billion gallons of jet fuel (equivalent to $8 billion) world wide. Therefore, the proposed thrust mechanism, if successfully developed, will save $25 billion for US airliners per year.

IX. Conclusion

In this paper, we studied the flapping propulsion problem. We showed several promising techniques to boost flapping propulsive efficiency beyond the current turbo fan engine technologies. In particular, we showed how large amplitude flapping in the stall regime may enhance propulsive efficiency. We also showed that, even in the small-disturbance linear range, allowing for a simultaneous oscillation in the flap deflection with pitching-plunging may enhance the propulsive efficiency by 20%. Therefore, we recommended allowing for more interactions with flow control mechanisms and provided a geometric control theoretic formulation to guide such nonlinear interactions. We also showed a room for capturing the free energy in the wing wake. Based on these premises, we proposed a new airplane concept, called the Flapping Tail Concept Airplane (FTCA), which is an airplane that is propelled by flapping its horizontal tail while its lift is generated in the conventional way using stationary wings. The Boeing 737-800 is used to demonstrate such a concept. The effect of the oscillating tail on the airplane flight mechanics is investigated and found to be minimal because of the too high oscillation frequency with respect to the flight mechanics natural modes. The paper serves as an initiator for several future investigations in the area.

X. Acknowledgments

The author would like to acknowledge the NSF grant CMMI-1635673.

References

[1]Rozhdestvensky, K. V. and Ryzhov, V. A., "Aerohydrodynamics of flapping-wing propulsors," *Progress in Aerospace Sciences*, Vol. 39, No. 8, 2003, pp. 585–633.

[2]DeLaurier, J. D., "The development and testing of a full-scale piloted ornithopter," *Canadian aeronautics and space*

journal, Vol. 45, No. 2, 1999, pp. 72–82.

[3]Mattingly, J. D. and Von Ohain, H., *Elements of propulsion: gas turbines and rockets*, American Institute of Aeronautics and Astronautics Reston, Virginia, 2006.

[4]Anderson, J. M., Streitlien, K., Barrett, D. S., and Triantafyllou, M. S., "Oscillating foils of high propulsive efficiency," *Journal of Fluid Mechanics*, Vol. 360, 1998, pp. 41–72.

[5]Garrick, I. E., "Propulsion of a flapping and oscillating airfoil," Tech. Rep. NACA-TR-567, 1937.

[6]Theodorsen, T., "General Theory of Aerodynamic Instability and the Mechanism of Flutter," Tech. Rep. 496, NACA, 1935.

[7]Schlichting, H. and Truckenbrodt, E., *Aerodynamics of the Airplane*, McGraw-Hill, 1979.

[8]Choi, J., Colonius, T., and Williams, D. R., "Surging and plunging oscillations of an airfoil at low Reynolds number," *Journal of Fluid Mechanics*, Vol. 763, 2015, pp. 237–253.

[9]Zakaria, M. Y., Taha, H. E., and Hajj, M. R., "Measurement and Modeling of Lift Enhancement on Plunging Airfoils: A Frequency Response Approach," *Journal of Fluids and Structures*, Vol. 69, 2017, pp. 187–208.

[10]Greenberg, J. M., "Airfoil in sinusoidal motion in a pulsating stream," Tech. rep., NACA, 1947.

[11]Wang, Z., "Vortex shedding and frequency selection in flapping flight," *Journal of Fluid Mechanics*, Vol. 410, 2000, pp. 323–341.

[12]Dickinson, M. H. and Gotz, K. C., "Unsteady Aerodynamic Performance of Model Wings at Low Reynolds Numbers." *Journal of Experimental Biology*, Vol. 174, No. 1, 1993, pp. 45–64.

[13]Wagner, H., "Uber die entstehung des dynamischen auftriebs von tragflugeln," *ZAMM*, Vol. 5, 1925.

[14]Heathcote, S. and Gursul, I., "Jet switching phenomenon for a periodically plunging airfoil," *Physics of Fluids (1994-present)*, Vol. 19, No. 2, 2007, pp. 027104.

[15]Cleaver, D. J., Wang, Z., and Gursul, I., "Bifurcating flows of plunging aerofoils at high Strouhal numbers," *Journal of Fluid Mechanics*, Vol. 708, 2012, pp. 349–376.

[16]Cleaver, D. J., Wang, Z., and Gursul, I., "Investigation of high-lift mechanisms for a flat-plate airfoil undergoing small-amplitude plunging oscillations," *AIAA journal*, Vol. 51, No. 4, 2013, pp. 968–980.

[17]Perkins, H. D., Wilson, J., and Raymer, D. P., "An Evaluation of Performance Metrics for High Efficiency Tube-and-Wing Aircraft Entering Service in 2030 to 2035," Tech. Rep. 217264, NASA, 2011.

[18]Dickinson, M. H., Lehmann, F.-O., and Sane, S. P., "Wing rotation and the aerodynamic basis of insect flight." *Science*, Vol. 284, No. 5422, 1999, pp. 1954–1960.

[19]Walker, J. A., "Rotational lift: something different or more of the same?" *Journal of Experimental Biology*, Vol. 205, No. 24, 2002, pp. 3783–3792.

[20]Kalman, R. E., Ho, Y.-C., and Narendra, K. S., "Controllability of linear dynamical systems," *Contributions to differential equations*, Vol. 1, No. 2, 1963, pp. 189–213.

[21]Baillieul, J. and Lehman, B., "Open-loop control using oscillatory inputs," *CRC Control Handbook*, 1996, pp. 967–980.

[22]Marsden, J. E., O'Reilly, O. M., Wicklin, F. J., and Zombros, B. W., "Symmetry, stability, geometric phases, and mechanical integrators," *Nonlinear Science Today*, Vol. 1, No. 1, 1991, pp. 4–11.

[23]Marsden, J. E., "Geometric foundations of motion and control," *Motion, Control, and Geometry: Proceedings of a Symposium, Board on Mathematical Science, National Research Council Education, National Academies Press, Washington, DC*, 1997, pp. 3–19.

[24]Murray, R. M. and Sastry, S. S., "Nonholonomic motion planning: Steering using sinusoids," *Automatic Control, IEEE Transactions on*, Vol. 38, No. 5, 1993, pp. 700–716.

[25]Liu, W., "Averaging theorems for highly oscillatory differential equations and iterated Lie brackets," *SIAM journal on control and optimization*, Vol. 35, No. 6, 1997, pp. 1989–2020.

[26]Liu, W., "An approximation algorithm for nonholonomic systems," *SIAM Journal on Control and Optimization*, Vol. 35, No. 4, 1997, pp. 1328–1365.

[27]Bullo, F. and Lewis, A. D., *Geometric control of mechanical systems*, Applied Mathematics, Springer-Verlag, Berlin, Germany, 2004.

[28]Jurdjevic, V., *Geometric control theory*, Cambridge university press, 1997.

[29]Nijmeijer, H. and Van der Schaft, A., *Nonlinear dynamical control systems*, Springer, 1990.

[30]Sastry, S., *Nonlinear systems: analysis, stability, and control*, Vol. 10, Springer New York, 1999.

[31]Monforte, J. C., *Geometric, control and numerical aspects of nonholonomic systems*, Springer, 2004.

[32]Walsh, G. C. and Sastry, S. S., "On reorienting linked rigid bodies using internal motions," *Robotics and Automation, IEEE Transactions on*, Vol. 11, No. 1, 1995, pp. 139–146.

[33]Sarychev, A., "Stability Criteria for Time-periodic Systems via High-order Averaging Techniques," *Nonlinear Control in the Year 2000*, Vol. 2 of *Lecture Notes in Control and Information Sciences*, Springer-Verlag, 2001, pp. 365–377.

[34]Vela, P. A., *Averaging and control of nonlinear systems (with application to biomimetic locomotion)*, Ph.D. thesis, California Institute of Technology, Pasadena, CA, May 2003.

[35]Bullo, F., "Averaging and vibrational control of mechanical systems," *SIAM Journal on Control and Optimization*, Vol. 41, No. 2, 2002, pp. 542–562.

[36]Agrachev, A. A. and Gamkrelidze, R. V., "The exponential representation of flows and the chronological calculus," *Matematicheskii Sbornik*, Vol. 149, No. 4, 1978, pp. 467–532.

[37]Taha, H. E., Woolsey, C. A., and Hajj, M. R., "Geometric Control Approach to Longitudinal Stability of Flapping Flight," *Journal of Guidance Control and Dynamics*, Vol. 39, No. 2, 2016, pp. 214–226.

[38]Taha, H. E. and Woolsey, C. A., "Geometric Control of a Flapping Plate," *Journal of Vibration and Control*, DOI: 10.1177/1077546313506924 2013, pp. 1–10.

[39]Taha, H. E., Woolsey, C. A., and Hajj, M. R., "A Geomteric Control Approach for Optimum Maneuverability of Flapping MAVs Near Hover," IEEE American Control Conference, Washington DC, Jun 2013, pp. 597–602.

[40]Hemati, M. S., Dawson, S. T. M., and Rowley, C. W., "Parameter-Varying Aerodynamics Models for Aggressive Pitching-Response Prediction," *AIAA Journal*, 2016, pp. 1–9.

[41]Liao, J. C., Beal, D. N., Lauder, G. V., and Triantafyllou, M. S., "The Kármán gait: novel body kinematics of rainbow trout swimming in a vortex street," *Journal of experimental biology*, Vol. 206, No. 6, 2003, pp. 1059–1073.

[42]Liao, J. C., "Neuromuscular control of trout swimming in a vortex street: implications for energy economy during the Karman gait," *Journal of Experimental Biology*, Vol. 207, No. 20, 2004, pp. 3495–3506.

[43]"Dead trout in flowing water," https://www.youtube.com/watch?v=_ZBWnhzYvts, Accessed: 01-17-2017.

[44]Nelson, R. C., *Flight stability and automatic control*, Vol. 2, WCB/McGraw Hill New York, 1998.

[45]Jones, R. T., "Operational treatment of the nonuniform lift theory to airplane dynamics," Tech. Rep. 667, NACA, 1938.

[46]Taha, H. E., Tahmasian, S., Woolsey, C. A., Nayfeh, A. H., and Hajj, M. R., "The Need for Higher-Order Averaging in the Stability Analysis of Hovering MAVs/Insects," Vol. 10, No. 1, pp. 016002, Selected in the Bioinspiration & Biomimetics Highlights of 2015.

[47]Hassan, A. M. and Taha, H. E., "Higher-Order Averaging Analysis of the Nonlinear Time-Periodic Dynamics of Hovering Insects/Flapping-Wing Micro-Air-Vehicles," IEEE Conference on Decision and Control, Las Vegas, NV, Dec 2016.

[48]Nayfeh, A. H. and Mook, D. T., *Nonlinear Oscillations*, John Wiley and Sons, Inc., 1979.

[49]Hassan, A. M. and Taha, H. E., "A combined Averaging-Shooting Approach for the Trim Analysis of Hovering Insects/Flapping-Wing Micro-Air-Vehicles," AIAA SciTech, Jan 2017, Selected as a finalist for the 2017 GNC Conference Graduate Student Paper Competition.

[50]Hassan, A. M. and Taha, H. E., "A Combined Averaging-Shooting Approach for the Analysis of Flapping Flight Dynamics," *Journal of Guidance Control and Dynamics*, Under Review.